THE JOURNAL OF PHYSICAL CHEMISTRY B
A JOURNAL OF THE AMERICAN CHEMICAL SOCIETY

pubs.acs.org/JPCB

Article

Influence of Solvents upon Diketopiperazine Formation of FPG_8K

Zhi-chao Zhang, Shannon A. Raab, David A. Hales,* and David E. Clemmer*

Cite This: https://dx.doi.org/10.1021/acs.jpcb.1c00269

Read Online

ACCESS | Metrics & More | Article Recommendations | Supporting Information

ABSTRACT: Ion mobility spectrometry (IMS) and mass spectrometry (MS) techniques were used to monitor diketopiperazine (DKP) formation from the peptide FPG_8K at multiple defined temperatures in methanol, ethanol, propanol, and water, with the motivation to study the effect of solvent polarity on spontaneous solution dissociation. The reaction rate increases with decreasing solvent polarity. The observed rates of *trans* → *cis* isomerization of Phe^1−Pro^2 and the *cis*-Pro^2 isomer dissociation result in the *cis* isomer growing in abundance relative to the *trans* isomer throughout the reaction in all solvents. Analysis of rate constants derived from the data using a sequential unimolecular kinetics model that includes hidden intermediate states yields transition state thermodynamic values for both *trans* → *cis* isomerization of Phe^1−Pro^2 and dissociation. The measured thermochemistry appears to be closely correlated with these solvents' dielectric constants: a lower solvent dielectric constant accelerates the reaction by reducing the enthalpic barrier, albeit with slight entropic restriction.

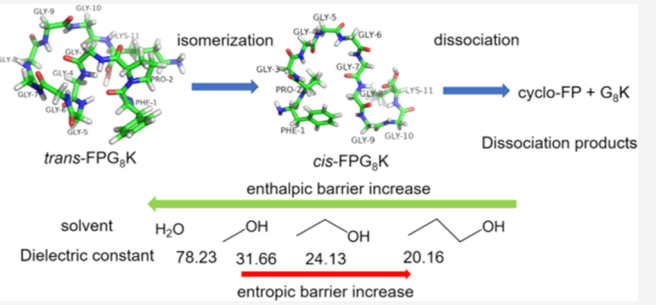

INTRODUCTION

Proteins and peptides can decompose during synthesis and storage through several spontaneous chemical reactions.[1,2] One of these reactions is diketopiperazine (2,5-dioxopiperazine, DKP) formation, which involves an N-terminal amine nucleophilic attack on the carbonyl carbon between the second and third amino acid residues, breaking the peptide chain and forming a cyclic peptide composed of the first two residues from the N-terminus and a truncated sequence of the peptide.[3−6] DKP formation happens especially when there is a proline residue at the second position from the N-terminus (i.e., penultimate proline). There are a few reports on this spontaneous degradation, including the dissociation of recombinant DNA-derived human growth hormone (rhGH) resulting in DKP and a truncated variant of rhGH;[7] degradation of the eleven-residue neuropeptide substance P in solution and solid forms;[8] and a recent report about self-cleavage of bradykinin at elevated temperature, which involves breaking the bond that is the most difficult to cleave enzymatically.[9]

Understanding the DKP formation reaction is of importance for other reasons as well. For example, it is a way of generating biologically active species throughout the body, such as cyclo(His−Pro).[10] Also, preventing intramolecular aminolysis is important for the storage of pharmaceutically important proteins and peptides since there are reports of decomposition of such compounds.[11,12] In addition, a recent finding by the Hunt group shows that a variety of MHC class I-associated phosphorylated peptides cause immune response.[13] These peptides have the potential to be used as novel vaccines for immunotherapy. However, many of these peptides contain a penultimate proline, which can lead to DKP formation and compromise the function of these peptides.

Several reports show that acids and bases, as well as buffer species, can influence the DKP formation rate in aqueous solution.[6,12,14] However, few reports analyzed the solvent effects on the DKP formation rate.[15,16] Also, the exact relationship between the rate of *trans* → *cis* isomerization of Xaa^1−Pro^2 and DKP formation has not been established. This is largely because almost all the previous research utilized techniques that were not able to separate the *cis* and *trans* isomers. The ion mobility spectrometry (IMS)−mass spectrometry (MS) technique has proven to be a useful tool to separate and analyze different conformations based on differences in molecules' overall mobility due to different collision cross sections.[17,18] Recent work used IMS−MS to analyze the dissociation kinetics of bradykinin and substance P,[9,19] in which different isomers due to proline *trans* → *cis* isomerization of the Xaa^1−Pro^2 bond are monitored during the degradation process. Analyzing the isomers from each species during dissociation provided evidence that at least three and four intermediates are involved in spontaneous solution dissociation of bradykinin and substance P, respectively. In

Received: January 11, 2021
Revised: February 26, 2021

each case, a configurationally coupled protonation process is observed as the penultimate proline that undergoes *trans* → *cis* isomerization, similarly to a previous Pro7 study.[20] Here, the peptide FPG_8K is used as a model to analyze DKP formation kinetics in four solvents at multiple defined temperatures. FPG_8K was selected because the conformations resulting from penultimate proline *trans* → *cis* isomerization have sufficiently different collision cross sections to be separable by IMS, thus enabling easy monitoring of changes in the *cis*/*trans* ratio of proline during degradation. Transition state thermochemistry values are also calculated for isomerization in all four solvents and for dissociation in three of the four solvents. This thermochemistry appears to be closely correlated with these solvents' dielectric constants. The implications of this are discussed below.

METHODS

Peptide Synthesis. Peptides are synthesized according to a traditional Fmoc solid-phase peptide synthesis procedure, as detailed elsewhere.[21] Briefly, 0.01 mmol Fmoc-Lys(Boc)-Wang resin is deprotected using piperidine/DMF (20% by volume). Then, the second amino acid from the C-terminus is activated using 3-(diethoxyphosphoryloxy)-1,2,3-benzotriazin-4(3H)-one (DEPBT) and *N*,*N*-diisopropylethylamine (DIEA) before mixing with the resin in 10 mL of DMF for ∼1.5 h. After mixing, the resulting product is washed with DMF, DCM, and MeOH three times each. This procedure is repeated until the peptide reaches the desired length. Cleavage from the resin is performed with TFA/H_2O/triisopropylsilane (95%/2.5%/2.5% V/V/V). The peptide is precipitated with diethyl ether and purified with HPLC.

Sample Preparation and Kinetics Experiment. A detailed description can be found in a previous paper.[9] Briefly, the peptide is dissolved into pure propanol, ethanol, methanol, or water to make 1 mM stock solutions which are stored at −20 °C. Stock solutions are diluted to 20 μM with 1% acetic acid (by volume) for use. The resulting alcohol solutions were then incubated at 65, 70, and 75 °C and tested periodically by IMS−MS. In water, we were able to monitor isomerization at 75 and 90 °C, but the dissociation process was too slow to be observed.

IMS Instrumentation. A home-built instrument in which a 2 m drift tube is coupled with a time-of-flight (TOF) mass spectrometer (see Supporting Information, Figure S14) is used to monitor the dissociation. Detailed descriptions of the instrument and theory appear elsewhere.[18,22−29] Briefly, ions are produced by nanoelectrospray in a NanoMate autosampler (Advion, Ithica, NY) and then transferred into the source region. Ions that are stored in the source funnel are periodically pulsed into the drift tube for separation based on their overall structural differences. The drift tube is filled with ∼3.0 torr (∼4.0 mbar) He buffer gas and operated under a weak electric field of roughly 10 V·cm^{-1}. The ions are analyzed using a TOF mass spectrometer after migrating through the 2 m drift tube. It is useful to convert the ion drift time t_D into the collisional cross section (CCS) (Ω, in Å^2) according to the following equation[25]

$$\Omega = \frac{(18\pi)^{1/2}}{16}\frac{ze}{(k_bT)^{1/2}}\left[\frac{1}{m_I}+\frac{1}{m_B}\right]^{1/2}\frac{t_DE}{L}\frac{760}{P}\frac{T}{273.2}\frac{1}{N} \quad (1)$$

where the relevant terms are ion charge (ze), Boltzmann's constant (k_b), mass of the ion (m_I), mass of the buffer gas (m_B), temperature of buffer gas (T), electric field value (E), drift tube length (L), pressure of buffer gas (P), and buffer gas neutral number density (N).

RESULTS AND DISCUSSION

Mass Spectral Data for $[FPG_8K + 2H]^{2+}$ Dissociation in Different Solvents. Figure 1 shows the mass spectra acquired

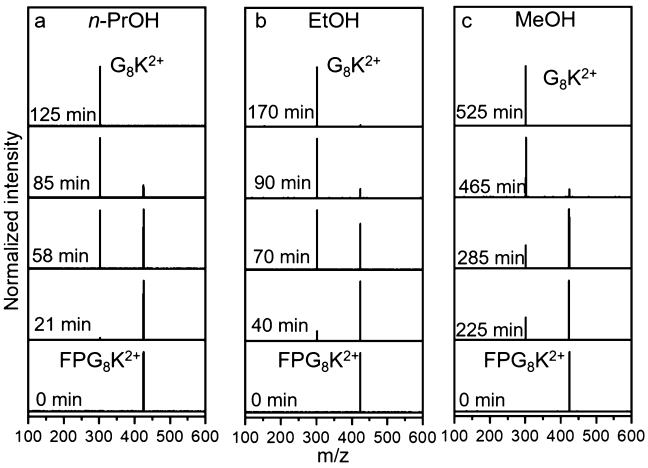

Figure 1. Peptide FPG_8K dissociation mass spectra in *n*-propanol (a), ethanol (b), and methanol (c) with 1% acetic acid (by volume) at 75 °C. Self-cleavage of the Pro^2−Gly^3 bond happens during the incubation. The dissociation half-lives are 48, 60, and 291 min in *n*-propanol, ethanol, and methanol, respectively. The dissociation is assumed to follow the DKP formation mechanism, as illustrated in Scheme 1.

Scheme 1. Cleavage Mechanism of Pro^2−Gly^3 by DKP Formation with Phe^1−Pro^2 in the *Cis* configuration[a]

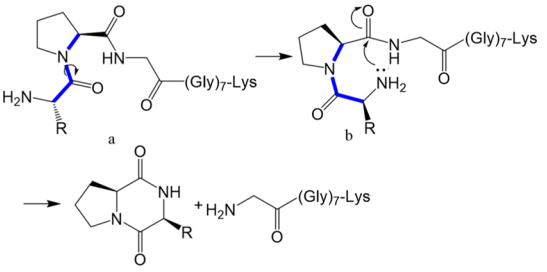

[a]The *cis* and *trans* isomers mentioned in this paper are b and a, respectively, when R = Phe.

after incubating FPG_8K in *n*-propanol, ethanol, and methanol (with 1% acetic acid) at 75 °C. In Figure 1a, peptide FPG_8K is incubated in *n*-propanol. At 0 min, there is one peak at m/z = 425.7 in the mass spectrum, corresponding to $[FPG_8K + 2H]^{2+}$. At 21 min, a new peak appears at m/z = 301.9, representing $[G_8K + 2H]^{2+}$. As time progresses, the $[FPG_8K + 2H]^{2+}$ peak decreases in abundance, while the $[G_8K + 2H]^{2+}$ peak grows in abundance. The degradation process is complete at around 125 min, when only $[G_8K + 2H]^{2+}$ remains. The dissociation half-life is around 48 min. Figure 1b,c shows peptide FPG_8K dissociation mass spectra in ethanol and methanol, respectively. Similar dissociation patterns are observed: as incubation time increases, the initial $[FPG_8K + 2H]^{2+}$ ion disappears, yielding the $[G_8K + 2H]^{2+}$ ion. The

https://dx.doi.org/10.1021/acs.jpcb.1c00269
J. Phys. Chem. B XXXX, XXX, XXX−XXX

dissociation half-lives in ethanol and methanol are 60 and 291 min, respectively. Peptide FPG_8K is also incubated in water. It takes 50 h for the dissociation to begin, which is much longer than in the other three solvents (see Supporting Information, Figure S1). It turns out that the FPG_8K dissociation rate increases with decreasing solvent polarity.

Collision Cross Section Distributions for $[FPG_8K + 2H]^{2+}$. The structural transition of FPG_8K can be directly monitored by examining IMS cross section distributions using the IMS−MS instrument. Pierson et al.[30] assigned proline isomers in bradykinin based on the fact that an alanine-substituted residue can only exist in the *trans* configuration. We took advantage of this approach here. Figure 2 shows the

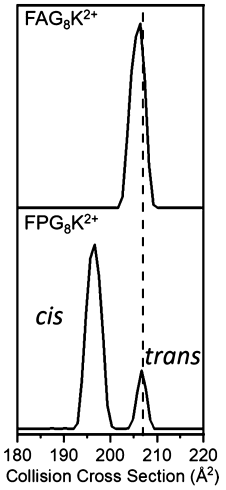

Figure 2. CCS distribution for $Pro^2 \rightarrow Ala$ of the $[FPG_8K + 2H]^{2+}$ ion. Distributions are obtained in ethanol with 1% acetic acid (by volume) from FPG_8K and FAG_8K. Alanine-substituted distribution is shown on top of $[FPG_8K + 2H]^{2+}$ as a comparison. Collision cross section distribution for the alanine-substituted peptide is corrected for the size difference between Ala and Pro.

CCS distribution of the peptide FPG_8K and its alanine-substituted analogue FAG_8K. The $^{DT}CCS_{He}$ values for the two conformations are $\Omega = 197 \pm 3$ and 207 ± 2 Å^2 for the peptide FPG_8K. Only the *trans* isomer is present in FAG_8K with $\Omega = 206 \pm 2$ Å^2, after correction for differences in the intrinsic size parameters between proline and alanine, as described previously.[31,32] Therefore, we assign the peak at $\Omega = 207 \pm 2$ Å^2 as the isomer with a *trans* penultimate proline, while the isomer at $\Omega = 197 \pm 3$ Å^2 has a *cis* penultimate proline.

Figure 3 shows the cross section distributions for FPG_8K in water, methanol, ethanol, and propanol. Both *cis* and *trans* isomers are observed, and the *cis* isomer is the major component. The percentages of the *cis* isomer are 88, 80, 75, and 60% in propanol, ethanol, methanol, and water, respectively. Although all these solvents favor the *cis* isomer overall, the amount of *trans* increases with solvent polarity.

An interesting question arises: is there a relationship between dissociation kinetics and the isomerization ratio? Figure 4 (top) shows the normalized intensity plots of FPG_8K isomerization and dissociation in *n*-PrOH, EtOH, MeOH, and H_2O at 75 °C. As dissociation progresses, both the *cis* and *trans* isomers of $[FPG_8K + 2H]^{2+}$ decrease in abundance, while the intensity of the fragment ion (i.e., $[G_8K + 2H]^{2+}$) increases. A previous study shows that peptides with a penultimate proline in the *trans* configuration cannot undergo the DKP formation

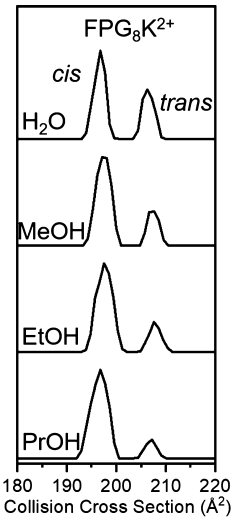

Figure 3. CCS distribution of the doubly charged peptide $[FPG_8K + 2H]^{2+}$ ions in water, propanol, ethanol, and methanol. Distributions were collected from IMS−MS instruments by integrating the drift bins for the m/z range of $[FPG_8K + 2H]^{2+}$ ions.

process;[33] therefore, the *trans* isomer of $[FPG_8K + 2H]^{2+}$ must undergo *trans* → *cis* isomerization of the Phe^1-Pro^2 bond before dissociation. The plot here shows that both the isomerization and fragmentation rates increase with decreasing polarity of the solvent.

Figure 4 (bottom) shows the percent of the *cis* isomer in the total distribution of $[FPG_8K + 2H]^{2+}$ during the degradation process in different solvents at 75 °C. The *trans* → *cis* isomerization of the Phe^1-Pro^2 bond continues even while the population of *cis* molecules is dissociating. The relative rates of the two steps result in the *cis* isomer growing in abundance relative to the *trans* isomer throughout the process. Unlike some protein folding processes in which the *trans* → *cis* isomerization of proline is the rate-limiting step,[34−36] isomerization and *cis* isomer dissociation of FPG_8K have comparable rates, with isomerization being somewhat faster than dissociation. The *cis* isomer abundance of the plots in Figure 4 increases with decreasing solvent polarity, implying that the effect of the solvent on the rates is stronger for isomerization than for fragmentation.

Characterizing the Dynamics and Pathways of FPG_8K Dissociation. In order to further understand the dynamics behind the dissociation, we modeled the experimental kinetics for several potential pathways and compared the sums of squares of the fitting residuals. This is conducted in a manner similar to that used in previous studies of dissociation of bradykinin and substance P.[9,19] Details of this type of fitting have been discussed previously.[37] We begin by considering the simplest pathway: FPG_8K with a *trans* penultimate proline undergoes *trans* → *cis* isomerization, while FPG_8K with a *cis* penultimate proline (both from the initial *cis* conformer population and the *cis* conformer converted from *trans*) dissociates to form cFP and G_8K, as shown by reactions 2 and 3

$$[\text{trans-}FPG_8K + 2H]^{2+} \rightarrow [\text{cis-}FPG_8K + 2H]^{2+} \quad (2)$$

$$[\text{cis-}FPG_8K + 2H]^{2+} \rightarrow [G_8K + 2H]^{2+} + \text{cFP} \quad (3)$$

In Figure 4 (top), the green lines show the best fits of these two models with the experimental data for methanol. These

https://dx.doi.org/10.1021/acs.jpcb.1c00269
J. Phys. Chem. B XXXX, XXX, XXX−XXX

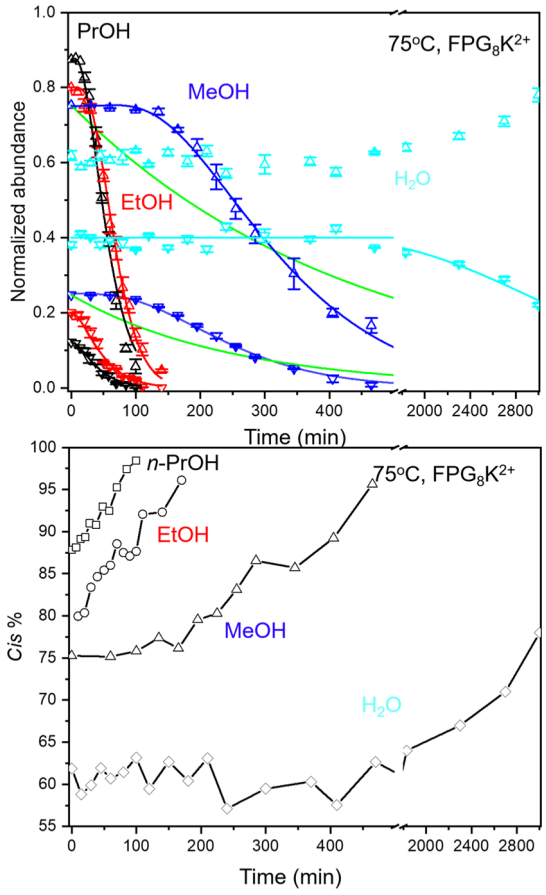

Figure 4. Top: Normalized abundances of the doubly charged peptide $[FPG_8K + 2H]^{2+}$ as incubation progresses in propanol (black), ethanol (red), methanol (blue), and water (cyan) at 75 °C. The hollow triangles and inverted triangles represent *cis* and *trans* $[FPG_8K + 2H]^{2+}$ ions, respectively. The abundance of $[FPG_8K + 2H]^{2+}$ ions' *cis* and *trans* conformations is extracted from the CCS distribution obtained by IMS−MS. Kinetic fits from several models are shown, including model 1 (for methanol, green curves) and the best-fitting model for each process (see Tables S1−S6 for details). Bottom: Percentage of *cis* relative to *trans* $[FPG_8K + 2H]^{2+}$ ions throughout the degradation process in propanol (rectangle), ethanol (circle), methanol (triangle), and water (diamond) at 75 °C. *Cis* % gradually increases as dissociation progresses to near 100% at the end of the dissociation. The rate of the *cis* % growth is proportional to the degradation rate. The entire dataset for the water system can be found in Supporting Information, Figure S16.

models fail to represent the general trend of the data. We compared 10 different model mechanisms for each process in each solvent. The sum of squares of the fitting residuals (ΣRSS) are listed with each candidate mechanism in Tables S1 (isomerization) and S2 (dissociation) for methanol. The single-step processes in 2 and 3 appear as model 1 in their respective tables. The sequential unimolecular models with three and four intermediates have the lowest ΣRSS and thus best reproduce the abundance profiles of *trans* → *cis* isomerization of the Phe^1-Pro^2 bond and *cis* isomer dissociation, respectively, as shown by the blue curves in Figure 4. The data for these two processes in ethanol and propanol are also best reproduced (ΣRSS at a minimum) by sequential unimolecular models, although with different numbers of unseen intermediates (see Supporting Information, Tables S3−S6). These intermediates are referred as unseen intermediates because they are not detected by IMS−MS but are derived from the best-fitting kinetics model.[9,37] FPG_8K *trans* → *cis* isomerization of the Phe^1-Pro^2 bond and *cis*-isomer dissociation require two and three intermediates in EtOH, while one and two intermediates yield the best fits to the 1-PrOH data. These fits for 75 °C are also shown in Figure 4, with data and fits for 70 and 65 °C found in Supporting Information, Figures S3−S7. The same type of figure and table for FPG_8K isomerization in water is shown in Table S7 and Figures S8 and S9, respectively.

The numbers of intermediates involved in dissociation in ethanol are similar to our previous study of bradykinin and substance P dissociation in the same solvent, in which, in total, at least three and four intermediates are involved in $BK(2H^+) \rightarrow BK_{(3-9)}(2H^+) + cRP(H^+)$ and $subP_{(3-11)}(2H^+) \rightarrow cKP(H^+) + subP_{(5-11)}$, respectively. In addition, one and zero intermediates are derived from the dissociation curves for penultimate proline *trans* → *cis* isomerization in bradykinin and substance P, which are close to the two intermediates found in this study for the same process in ethanol. A previous Pro13 study shows that the all-*cis*-configured right-handed helical PPI conformer can undergo *trans* → *cis* isomerization of each peptide bond into an all-*trans*-configured PPII structure, during which six distinct long-lived intermediates are observed.[38] The proline chain in HisPro13 undergoes the same process via a cooperative two-state transition with ∼15 unseen intermediates.[37] These results suggest that intermediate conformations are likely inherent in proline *trans* → *cis* isomerization.

Transition State Thermodynamics. After fitting the data at various temperatures, Arrhenius plots are generated for FPG_8K *trans* → *cis* isomerization of the Phe^1-Pro^2 bond and *cis*-FPG_8K dissociation in each solvent by plotting the natural log of the rate constant against inverse temperature according to eq 4.

Table 1. Summary of Transition State Thermodynamic Values at 298 K for FPG_8K *Trans* → *Cis* Isomerization and *cis*-FPG_8K Dissociation in Different Solvents

solvents	process[a]	$\Delta G^{\ddagger}$ (kJ·mol^{-1})	$\Delta H^{\ddagger}$ (kJ·mol^{-1})	$\Delta S^{\ddagger}$ (J·mol^{-1}·K^{-1})	E_a (kJ·mol^{-1})
n-PrOH	*trans* → *cis* (1)	100.1 ± 2.1	104.3 ± 1.6	14.1 ± 4.7	101.8 ± 1.6
n-PrOH	dissociation (2)	99.4 ± 2.4	105.6 ± 2.2	20.9 ± 3.5	103.1 ± 2.2
EtOH	*trans* → *cis* (2)	100.5 ± 1.1	106.0 ± 0.5	18.4 ± 3.4	103.5 ± 0.5
EtOH	dissociation (3)	99.9 ± 3.7	109.5 ± 3.4	31.9 ± 5.5	107.0 ± 3.4
MeOH	*trans* → *cis* (3)	103.8 ± 1.7	110.0 ± 1.3	21.0 ± 3.7	107.6 ± 1.3
MeOH	dissociation (4)	104.1 ± 0.4	116.4 ± 0.2	41.1 ± 1.1	113.9 ± 0.2
H_2O	*trans* → *cis* (7)	110.0 ± 3.2	120.4 ± 2.5	35.0 ± 6.7	117.9 ± 2.5

[a]The number in the parenthesis represents the number of unseen intermediates derived from the best-fitting model.

https://dx.doi.org/10.1021/acs.jpcb.1c00269
J. Phys. Chem. B XXXX, XXX, XXX−XXX

$$\ln(k) = \frac{-E_a}{R}\cdot\frac{1}{T} + \ln(A) \quad (4)$$

(Supporting Information, Figures S10−S13) activation energy (E_a) and the pre-exponential factor (A) are determined from the slope and y-intercept, respectively, of the best-fitting line. Transition state theory then allows us to parse out the contributions of $\Delta H^{\ddagger}$ and entropy ($\Delta S^{\ddagger}$) to the transition barriers in each solvent based on eqs 5 and 6

$$\Delta H^{\ddagger} = E_a + RT \quad (5)$$

$$A = \frac{ek_BT}{h}e^{\Delta S^{\ddagger}/R} \quad (6)$$

$$\Delta G^{\ddagger} = \Delta H^{\ddagger} - T\Delta S \quad (7)$$

where h is Planck's constant, k_B is Boltzmann's constant, R is the gas constant, T is temperature of the reaction, and e is Euler's number. We calculated the Gibbs free energy according to eq 7 for each transition state ($\Delta G^{\ddagger}$) from $\Delta H^{\ddagger}$ and $\Delta S^{\ddagger}$ determined here. The derived values are shown in Table 1. The consecutive-step analysis assumes identical rate constants for all steps through a group of unseen intermediates that lead to an observed change—either isomerization or dissociation—so these are single-step barriers.

The derived enthalpy of activation for dissociation is higher in each solvent than that for the isomerization step, and the difference grows with solvent polarity. In propanol, the $\Delta H^{\ddagger}$ values are essentially the same for the two steps in that the uncertainty ranges of the two values overlap. These differences easily exceed the uncertainty ranges for ethanol and methanol, so the solvent polarity effect is clearly real. Not only is each barrier higher for the dissociation step than for *trans* → *cis* isomerization of Phe[1]−Pro[2] but also dissociation involves more consecutive barriers (due to the unseen intermediates) in all three solvents.

The entropy of activation for both steps depends similarly on solvent polarity. We find that the value of $\Delta S^{\ddagger}$ for both the isomerization and dissociation steps increases with solvent polarity. In addition, the difference between $\Delta S^{\ddagger}$ for isomerization and dissociation in a given solvent increases with solvent polarity. Unlike enthalpy, although, a higher entropy value eases the process. The higher the value of $\Delta S^{\ddagger}$, the greater the loss of molecular order as the combined peptide−solvent system approaches the transition state. The dissociation transition state is looser than that of isomerization: the channel on the potential energy surface through which a *cis* conformer dissociates is less entropically restrictive than that through which *trans* to *cis* isomerization proceeds. In other words, in a potential energy diagram, a broader range of conformations is compatible with crossing the transition for *cis* conformer dissociation than for a *trans* isomer isomerization. In each solvent, the uncertainty range of $\Delta G^{\ddagger}$ for *trans* → *cis* isomerization overlaps with that for dissociation, so the two values are statistically indistinguishable. The barriers for *trans* → *cis* isomerization at penultimate proline determined here are similar to previously reported values for other peptides.[9,39] While the $\Delta H^{\ddagger}$ values account for the bulk of each free energy barrier, the entropic easing effect is the largest where the enthalpic barriers are the largest. This results in both the similarity of $\Delta G^{\ddagger}$ for isomerization and dissociation in a given solvent and the fact that all seven $\Delta G^{\ddagger}$ values across the three solvents are in the same neighborhood. There appears to be an enthalpy and entropy compensation that results in similar free energy barriers for each step, as observed in previous research.[40−44]

Of these three solvents, FPG_8K degradation kinetics is the fastest in propanol. Propanol also yields the smallest number of intermediates involved in both FPG_8K *trans* → *cis* isomerization and *cis*-FPG_8K dissociation processes. We can make sense of this by noting that the strength of hydrogen bonding interactions between the peptide and solvent should increase with solvent polarity. Therefore, a more polar solvent requires more energy for the peptide to undergo structural change, whether *trans* → *cis* isomerization or *cis* conformation dissociation. This manifests as a larger $\Delta H^{\ddagger}$ in a more polar solvent. The tighter solvent−peptide interactions in a more polar solvent also may play into the higher number of hidden intermediate states, as the peptide and surrounding solvent molecules both rearrange on the way to completing each of the two observable steps. The peptide−solvent and solvent−solvent interactions that must be overcome as the peptide rearranges have a greater initial ordering effect in a solvent that makes stronger hydrogen bonds. The observed trend of higher $\Delta S^{\ddagger}$ in a more polar solvent thus seems more likely to grow out of greater order in the potential well before the transition barrier than from additional disorder in the transition state itself.

Transition State Thermochemistry and the Dielectric Constant of the Solvent. Because of the changes in thermochemistry observed with variations in solvent polarity, it is interesting to consider the relationship of the measured thermochemistry and the dielectric constants of the solvents. Plots of transition state thermochemistry versus dielectric constant for both isomerization and dissociation of the peptide FPG_8K are shown in Figures 5 and 6, respectively. The corresponding regression values and uncertainties are listed in Table 2. Transition state thermochemistry appears to be correlated with the dielectric constant of the solvent. Both $\Delta H^{\ddagger}$ and $T\Delta S^{\ddagger}$ increase with increases in the dielectric constant.

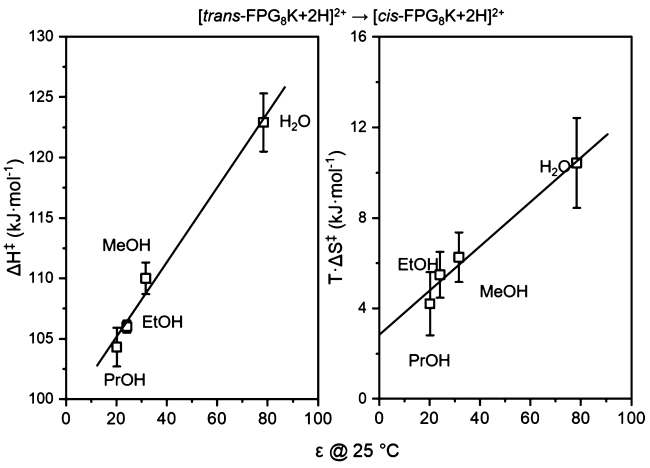

Figure 5. $\Delta H^{\ddagger}$ and $T\Delta S^{\ddagger}$ *vs* dielectric constant (values are used at 25 °C) diagram for the isomerization step of each solvent system investigated. The correlation equations for $\Delta H^{\ddagger}$ *vs* dielectric constant and $T\Delta S^{\ddagger}$ *vs* dielectric constant are $y = 0.26x + 99.96$ and $y = 0.99x + 2.79$, respectively. Each value is the average of triplicate measurements, and error bars represent the standard deviation about the mean. T is 298.15 K.

https://dx.doi.org/10.1021/acs.jpcb.1c00269
J. Phys. Chem. B XXXX, XXX, XXX−XXX

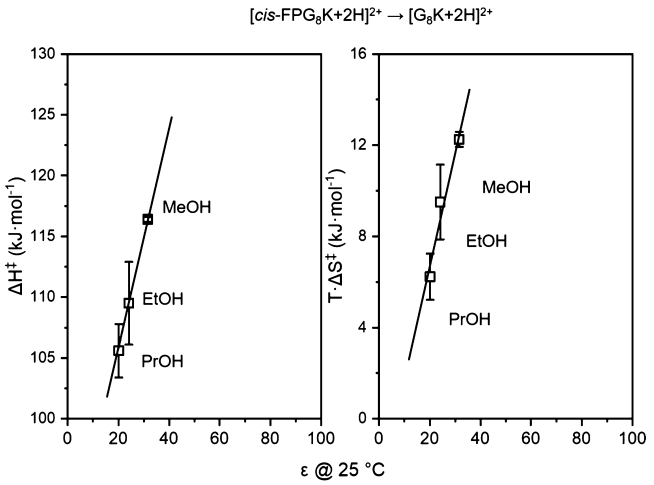

Figure 6. $\Delta H^{\ddagger}$ and $T\Delta S^{\ddagger}$ *vs* dielectric constant (values are used at 25 °C) diagram for the dissociation step of each solvent system investigated. The correlation equation for $\Delta H^{\ddagger}$ *vs* dielectric constant and $T\Delta S^{\ddagger}$ *vs* dielectric constant are $y = 0.94x + 87.80$ and $y = 0.50x - 3.40$, respectively. Each value is the average of triplicate measurements, and error bars represent the standard deviation about the mean. T is 298.15 K.

Table 2. Regression Values and Uncertainties of Correlation of $\Delta H^{\ddagger}$ and $T\Delta S^{\ddagger}$ *Versus* Dielectric Constant for Isomerization and Dissociation Processes

	process	equation	R-square
$\Delta H^{\ddagger}$ *vs* ε	isomerization	$y = 0.26x + 99.96$	0.975
$\Delta H^{\ddagger}$ *vs* ε	dissociation	$y = 0.94x + 87.80$	1.000
$T\Delta S^{\ddagger}$ *vs* ε	isomerization	$y = 0.99x + 2.79$	0.974
$T\Delta S^{\ddagger}$ *vs* ε	dissociation	$y = 0.50x - 3.40$	0.949

In Figures 5 and 6, trend lines are derived based on transition state enthalpy and entropy values. Extrapolation to $\varepsilon = 1$ yields transition state thermochemistry corresponding to vacuum: for the isomerization step, $\Delta H^{\ddagger}$, $\Delta S^{\ddagger}$, and $\Delta G^{\ddagger}$ are 100.2 kJ·mol^{-1}, 9.7 J·mol^{-1}·K^{-1}, and 97.3 kJ·mol^{-1}, respectively, and for the dissociation step, $\Delta H^{\ddagger}$, $\Delta S^{\ddagger}$, and $\Delta G^{\ddagger}$ are 88.7 kJ·mol^{-1}, −9.7 J·mol^{-1}·K^{-1}, and 91.6 kJ·mol^{-1}, respectively. These results represent the contributions from the peptide itself to the total transition state thermochemistry. The values here suggest that both steps are enthalpically disfavored. However, these extrapolations to vacuum predict $\Delta H^{\ddagger}$ for isomerization to be higher than for dissociation, which is the opposite of our solution-phase results. In addition, while both steps are entropically favored in solution, in vacuum, the dissociation step is predicted to be restricted entropically. This comparison is also reversed from the solution-phase results. A negative $\Delta S\ddagger$ makes sense for dissociation in that the reaction requires a precise attack of an amine nitrogen on a carbonyl carbon. These trend lines might also allow predictions about the reaction rate and transition state thermochemistry in biological environments with varying local dielectric characteristics. It is worth mentioning that the correlation curves are different with or without the derived transition state thermochemistry values of water for the isomerization step. The derived values for the peptide isomerization without including the data with water as a solvent are as follows: $\Delta H^{\ddagger}$, $\Delta S^{\ddagger}$, and $\Delta G^{\ddagger}$ values are 94.4 kJ·mol^{-1}, 4.10 J·mol^{-1}·K^{-1}, and 93.3 kJ·mol^{-1}, respectively. Although these values vary once, we include the data associated with water as the solvent, the general thermochemical trends remain consistent and this does not change our overall conclusions.

Both $\Delta H^{\ddagger}$ and $T\Delta S^{\ddagger}$ grow with increasing dielectric constant. This means the entropic barrier is eased as the enthalpic barrier grows. Conversely, the dissociation in the solvent with a lower dielectric constant is favored largely by lowering the enthalpic barrier, while slightly increasing the entropic barrier. This opposed trend of entropic and enthalpic barriers with a dielectric constant is reminiscent of enzyme behavior. The dielectric environment of the active pocket of an enzyme depends on which residues are present but will, in general, differ significantly from the dielectric environment of the solvent, which could contribute to high catalytic activity.[45−47] This difference of permittivity leads to a decrease in activation energy at the expense of entropic restriction, which parallels the behavior we see here with changes in solvent dielectric constant.

The fact that the fragmentation rate increases with decreasing dielectric constant leads us to offer a final suggestion. In the nonpolar environment of a biological membrane, the DKP formation rate should be faster than the same reaction under aqueous conditions. This implies that as peptides are screened for possible drug or antigen use *in vivo*, susceptibility to DKP formation should be considered and, if possible, such studies should consider a variety of environments.

Proton Concentration from Acetic Acid Dissociation in Different Solvent. Considering the fact that DKP formation reaction is influenced by the protonation of the N-terminus (a free amino group is necessary for the nucleophilic attack), the dissociation of acetic acid in different solvents, which contributes to the donation of protons to the solvent, could affect dissociation. The pK_a values of acetic acid in PrOH, EtOH, MeOH, and H_2O are 10.45, 10.32, 9.63, and 4.75, respectively.[48−50] Since 1% acetic acid (17.5×10^4 μM) is added to each solution, the calculated [H$^+$] in H_2O, MeOH, EtOH, and PrOH are 5.5×10^{-4}, 2.0×10^{-6}, 9.2×10^{-7}, and 7.9×10^{-7} M, respectively. The correlation between log[H$^+$] and the solvent dielectric constant appears to be linear (shown in Figure S15). The concentration of the peptide FPG_8K is 20 μM, ∼0.04, 10, 22, and 25 times the concentration of [H$^+$] in H_2O, MeOH, EtOH, and PrOH, respectively. Overall, we see that this trend is opposed to experimental finding, suggesting that excess protons have little if any influence on this system.

CONCLUSIONS

IMS−MS techniques were used to investigate the dissociation kinetics of FPG_8K in different solvents at multiple defined temperatures. The CCS distribution shows that two conformations in solution result from the peptide's *trans* → *cis* isomerization at proline. Using IMS−MS, we are able to monitor changes in abundance of the *cis* and *trans* isomers alongside the dissociation process. We found that there are two processes involved in the dissociation: *trans* → *cis* isomerization and *cis* isomer degradation. We found that DKP formation is more rapid in less polar solvents. Decreased solvent polarity also enhances the preference for the *cis* conformation over *trans* at the penultimate proline and speeds up the *trans* → *cis* isomerization process. By monitoring the dissociation process at multiple temperatures and modeling the dissociation pathway, we found that a number of unseen intermediates are involved in both isomerization and

https://dx.doi.org/10.1021/acs.jpcb.1c00269
J. Phys. Chem. B XXXX, XXX, XXX−XXX

dissociation. This modeling also allowed us to determine transition state thermodynamic values. There appears to be a strong correlation between the dielectric constant and transition state enthalpy and entropy. The solvent with a lower dielectric constant speeds up the reaction by lowering the enthalpic barrier although slightly increasing the entropic barrier. The Gibbs free energy of activation in all the solvents are primarily controlled by transition state enthalpy.

■ ASSOCIATED CONTENT

Supporting Information

The Supporting Information is available free of charge at https://pubs.acs.org/doi/10.1021/acs.jpcb.1c00269.

Dissociation mass spectra of FPG_8K in water; kinetics data of $[FPG_8K + 2H]^{2+}$ in different solutions under multiple elevated temperatures; Arrhenius plots for the peptide FPG_8K in different solutions; schematic diagram of a 2 m instrument; $\log[H^+]$ *versus* dielectric constant diagram; percentage of cis relative to the trans isomer throughout the degradation process in water; and residue sums of square values for FPG_8K dissociation and *trans* → *cis* isomerization processes in different solutions (PDF)

■ AUTHOR INFORMATION

Corresponding Authors

David A. Hales − *Department of Chemistry, Indiana University, Bloomington, Indiana 47401, United States; Department of Chemistry, Hendrix College, Conway, Arkansas 72032, United States*; Email: hales@hendrix.edu

David E. Clemmer − *Department of Chemistry, Indiana University, Bloomington, Indiana 47401, United States*; orcid.org/0000-0003-4039-1360; Email: clemmer@indiana.edu

Authors

Zhi-chao Zhang − *Department of Chemistry, Indiana University, Bloomington, Indiana 47401, United States*

Shannon A. Raab − *Department of Chemistry, Indiana University, Bloomington, Indiana 47401, United States*

Complete contact information is available at: https://pubs.acs.org/10.1021/acs.jpcb.1c00269

Notes

The authors declare no competing financial interest.

■ ACKNOWLEDGMENTS

This work is supported by funds from the National Institutes of Health grant 5R01GM121751-03 (D.E.C.), the Robert and Marjorie Mann Graduate Research Fellowship (Z.Z. and S.A.R.) from Indiana University, and a Faculty Project Grant from Hendrix College (D.A.H.). The authors acknowledge Navneet Sahota, Dr. Daniel Fuller, and Dr. Chris Conant for help, and NS, CRC, and DRF were supported by fellowships from the Robert and Marjorie Mann Chair.

■ REFERENCES

(1) Manning, M. C.; Chou, D. K.; Murphy, B. M.; Payne, R. W.; Katayama, D. S. Stability of protein pharmaceuticals: an update. *Pharm. Res.* **2010**, *27*, 544−575.

(2) Manning, M. C.; Patel, K.; Borchardt, R. T. Stability of protein pharmaceuticals. *Pharm. Res.* **1989**, *06*, 903−918.

(3) Capasso, S.; Vergara, A.; Mazzarella, L. Mechanism of 2,5-Dioxopiperazine Formation. *J. Am. Chem. Soc.* **1998**, *120*, 1990−1995.

(4) Marsden, B. J.; Nguyen, T. M.; Schiller, P. W. Spontaneous degradation via diketopiperazine formation of peptides containing a tetrahydroisoquinoline-3-carboxylic acid residue in the 2-position of the peptide sequence. *Int. J. Pept. Protein Res.* **1993**, *41*, 313−316.

(5) Steinberg, S. M.; Bada, J. L. Peptide decomposition in the neutral pH region via the formation of diketopiperazines. *J. Org. Chem.* **1983**, *48*, 2295−2298.

(6) Beyermann, M.; Bienert, M.; Niedrich, H.; Carpino, L. A.; Sadat-Aalaee, D. Rapid continuous peptide synthesis via FMOC amino acid chloride coupling and 4-(aminomethyl)piperidine deblocking. *J. Org. Chem.* **1990**, *55*, 721−728.

(7) Battersby, J. E.; Hancock, W. S.; Canova-Davis, E.; Oeswein, J.; O'Connor, B. Diketopiperazine formation and N-terminal degradation in recombinant human growth hormone. *Int. J. Pept. Protein Res.* **1994**, *44*, 215−222.

(8) Kertscher, U.; Bienert, M.; Krause, E.; Sepetov, N. F.; Mehlis, B. Spontaneous chemical degradation of substance P in the solid phase and in solution. *Int. J. Pept. Protein Res.* **1993**, *41*, 207−111.

(9) Fuller, D. R.; Conant, C. R.; El-Baba, T. J.; Brown, C. J.; Woodall, D. W.; Russell, D. H.; Clemmer, D. E. Conformationally regulated peptide bond cleavage in bradykinin. *J. Am. Chem. Soc.* **2018**, *140*, 9357−9360.

(10) Møss, J.; Bundgaard, H. Kinetics and mechanism of the facile cyclization of histidyl-prolineamide to cyclo (His-Pro) in aqueous solution and the competitive influence of human plasma. *J. Pharm. Pharmacol.* **1990**, *42*, 7−12.

(11) Oyler, A. R.; Naldi, R. E.; Lloyd, J. R.; Graden, D. A.; Shaw, C. J.; Cotter, M. L. Characterization of the solution degradation products of histrelin, a gonadotropin releasing hormone (LH/RH) agonist. *J. Pharm. Sci.* **1991**, *80*, 271−275.

(12) Straub, J. A.; Akiyama, A.; Parmar, P.; Musso, G. F. Chemical pathways of degradation of the bradykinin analog, RMP-7. *Pharm. Res.* **1995**, *12*, 305−308.

(13) Cobbold, M.; De La Peña, H.; Norris, A.; Polefrone, J. M.; Qian, J.; English, A. M.; Cummings, K. L.; Penny, S.; Turner, J. E.; Cottine, J.; et al. MHC Class I-associated hosphopeptides are the targets of memory-like immunity in leukemia. *Sci. Transl. Med.* **2013**, *5*, 203ra125.

(14) Sepetov, N. F.; Krymsky, M. A.; Ovchinnikov, M. V.; Bespalova, Z. D.; Isakova, O. L.; Soucek, M.; Lebl, M. Rearrangement, racemization and decomposition of peptides in aqueous solution. *Pept. Res.* **1991**, *4*, 308−313.

(15) Capasso, S.; Mazzarella, L. Activation of diketopiperazine formation by alkylammonium carboxylate salts and aprotic dipolar protophobic solvents. *Peptides* **1998**, *19*, 389−391.

(16) Capasso, S.; Mazzarella, L. Solvent effects on diketopiperazine formation from N-terminal peptide residues. *J. Chem. Soc., Perkin Trans. 2* **1999**, 329−332.

(17) Clemmer, D. E.; Jarrold, M. F. Ion mobility measurements and their applications to clusters and biomolecules. *J. Mass Spectrom.* **1997**, *32*, 577−592.

(18) Bohrer, B. C.; Merenbloom, S. I.; Koeniger, S. L.; Hilderbrand, A. E.; Clemmer, D. E. Biomolecule analysis by ion mobility spectrometry. *Annu. Rev. Anal. Chem.* **2008**, *1*, 293−327.

(19) Conant, C. R.; Fuller, D. R.; El-Baba, T. J.; Zhang, Z.; Russell, D. H.; Clemmer, D. E. Substance P in solution: trans-to-cis configurational changes of penultimate prolines initiate non-enzymatic peptide bond cleavages. *J. Am. Soc. Mass Spectrom.* **2019**, *30*, 919−931.

(20) Shi, L.; Holliday, A. E.; Khanal, N.; Russell, D. H.; Clemmer, D. E. Configurationally-coupled protonation of polyproline-7. *J. Am. Chem. Soc.* **2015**, *137*, 8680−8683.

(21) Coin, I.; Beyermann, M.; Bienert, M. Solid-phase peptide synthesis: from standard procedures to the synthesis of difficult sequences. *Nat. Protoc.* **2007**, *2*, 3247−3256.

(22) Koeniger, S. L.; Merenbloom, S. I.; Sevugarajan, S.; Clemmer, D. E. Transfer of structural elements from compact to extended states in unsolvated ubiquitin. *J. Am. Chem. Soc.* **2006**, *128*, 11713−11719.
(23) Merenbloom, S. I.; Koeniger, S. L.; Valentine, S. J.; Plasencia, M. D.; Clemmer, D. E. IMS−IMS and IMS−IMS−IMS/MS for separating peptide and protein fragment ions. *Anal. Chem.* **2006**, *78*, 2802−2809.
(24) Mesleh, M. F.; Hunter, J. M.; Shvartsburg, A. A.; Schatz, G. C.; Jarrold, M. F. Structural information from ion mobility measurements: effects of the long-range potential. *J. Phys. Chem.* **1996**, *100*, 16082−16086.
(25) Mason, E. A.; McDaniel, E. W. *Transport Properties of Ions in Gases*; John Wiley & Sons: Hoboken, NJ, 1988.
(26) Revercomb, H. E.; Mason, E. A. Theory of plasma chromatography/gaseous electrophoresis. Review. *Anal. Chem.* **1975**, *47*, 970−983.
(27) Wyttenbach, T.; von Helden, G.; Batka, J. J.; Carlat, D.; Bowers, M. T. Effect of the long-range potential on ion mobility measurements. *J. Am. Soc. Mass Spectrom.* **1997**, *8*, 275−282.
(28) McLean, J. A.; Ruotolo, B. T.; Gillig, K. J.; Russell, D. H. Ion mobility-mass spectrometry: a new paradigm for proteomics. *Int. J. Mass Spectrom.* **2005**, *240*, 301−315.
(29) Kanu, A. B.; Dwivedi, P.; Tam, M.; Matz, L.; Hill, H. H., Jr Ion mobility-mass spectrometry. *J. Mass Spectrom.* **2008**, *43*, 1−22.
(30) Pierson, N. A.; Chen, L.; Russell, D. H.; Clemmer, D. E. Cis−Trans Isomerizations of proline residues are key to bradykinin conformations. *J. Am. Chem. Soc.* **2013**, *135*, 3186−3192.
(31) Valentine, S. J.; Counterman, A. E.; Hoaglund-Hyzer, C. S.; Clemmer, D. E. Intrinsic amino acid size parameters from a series of 113 lysine-terminated tryptic digest peptide ions. *J. Phys. Chem. B* **1999**, *103*, 1203−1207.
(32) Srebalus Barnes, C. A.; Clemmer, D. E. Assessing intrinsic side chain interactions between i and i + 4 residues in solvent-free peptides: a combinatorial gas-phase approach[†]. *J. Phys. Chem. A* **2003**, *107*, 10566−10579.
(33) Fuller, D. R.; Conant, C. R.; El-Baba, T. J.; Brown, C. J.; Woodall, D. W.; Russell, D. H.; Clemmer, D. E. Conformationally regulated peptide bond cleavage in bradykinin. *J. Am. Chem. Soc.* **2018**, *140*, 9357−9360.
(34) Brandts, J. F.; Halvorson, H. R.; Brennan, M. Consideration of the possibility that the slow step in protein denaturation reactions is due to cis-trans isomerism of proline residues. *Biochemistry* **1975**, *14*, 4953−4963.
(35) Brandts, J. F.; Brennan, M.; Lung-Nan Lin, L.-N. Unfolding and refolding occur much faster for a proline-free proteins than for most proline-containing proteins. *Proc. Natl. Acad. Sci. U.S.A.* **1977**, *74*, 4178−4181.
(36) Lin, L.-N.; Brandts, J. F. Further evidence suggesting that the slow phase in protein unfolding and refolding is due to proline isomerization: a kinetic study of carp parvalbumins. *Biochemistry* **1978**, *17*, 4102−4110.
(37) El-Baba, T. J.; Kim, D.; Rogers, D. B.; Khan, F. A.; Hales, D. A.; Russell, D. H.; Clemmer, D. E. Long-lived intermediates in a cooperative two-state folding transition. *J. Phys. Chem. B* **2016**, *120*, 12040−12046.
(38) Shi, L.; Holliday, A. E.; Shi, H.; Zhu, F.; Ewing, M. A.; Russell, D. H.; Clemmer, D. E. Characterizing intermediates along the transition from polyproline I to polyproline II using ion mobility spectrometry-mass spectrometry. *J. Am. Chem. Soc.* **2014**, *136*, 12702−12711.
(39) Shi, L.; Holliday, A. E.; Glover, M. S.; Ewing, M. A.; Russell, D. H.; Clemmer, D. E. Ion mobility-mass spectrometry reveals the energetics of intermediates that guide polyproline folding. *J. Am. Soc. Mass Spectrom.* **2016**, *27*, 22−30.
(40) Liu, L.; Guo, Q.-X. Isokinetic relationship, isoequilibrium relationship, and enthalpy−entropy compensation. *Chem. Rev.* **2001**, *101*, 673−696.
(41) Pan, A.; Biswas, T.; Rakshit, A. K.; Moulik, S. P. Enthalpy−entropy compensation (EEC) effect: a revisit. *J. Phys. Chem. B* **2015**, *119*, 15876−15884.
(42) Sharp, K. Entropy–enthalpy compensation: Fact or artifact? *Protein Sci.* **2001**, *10*, 661−667.
(43) Chodera, J. D.; Mobley, D. L. Entropy-enthalpy compensation: role and ramifications in biomolecular ligand recognition and design. *Annu. Rev. Biophys.* **2013**, *42*, 121−142.
(44) El-Baba, T. J.; Fuller, D. R.; Hales, D. A.; Russell, D. H.; Clemmer, D. E. Solvent mediation of peptide conformations: polyproline structures in water, methanol, ethanol, and 1-propanol as determined by ion mobility spectrometry-mass spectrometry. *J. Am. Soc. Mass Spectrom.* **2019**, *30*, 77−84.
(45) Krishtalik, L. The specific features of enzyme as a polar medium and their role in the mechanism of the enzymatic process. *Mol. Biol.* **1974**, *8*, 91−99.
(46) Krishtalik, L. I. Globule size and the activation energy of an enzymatic process. *Mol. Biol.* **1979**, *13*, 577−581.
(47) Krishtalik, L. I. Catalytic acceleration of reactions by enzymes. Effect of screening of a polar medium by a protein globule. *J. Theor. Biol.* **1980**, *86*, 757−771.
(48) Goffredi, M.; Shedlovsky, T. Electrolytic conductance in alcohol-water mixtures. V. Ionization constant of acetic acid in 1-propanol-water mixtures at 15, 25, and 35.degree. *J. Phys. Chem. B* **1967**, *71*, 4436−4442.
(49) Shedlovsky, T.; Kay, R. L. The ionization constant of acetic acid in water−methanol mixtures at 25° from conductance measurements. *J. Phys. Chem. B* **1956**, *60*, 151−155.
(50) Grunwald, E.; Berkowitz, B. J. The measurement and correlation of acid dissociation constants for carboxylic acids in the system ethanol−water. Activity Coefficients and Empirical Activity Functions[1a]. *J. Am. Chem. Soc.* **1951**, *73*, 4939−4944.

https://dx.doi.org/10.1021/acs.jpcb.1c00269
J. Phys. Chem. B XXXX, XXX, XXX−XXX